This is a previous version of the article published in Chinese Journal of Catalysis. 2022, 43(11): 2837-2849. https://doi.org/10.1016/S1872-2067(22)64138-X

Understanding Surface Charge Effects in Electrocatalysis. Part 2: Hydrogen Peroxide Reactions at Platinum

Jun Huang,*[,a] Victor Climent,[b] Axel Groß,[a,c] Juan Feliu*[,b]

[a] Institute of Theoretical Chemistry, Ulm University, 89069 Ulm, Germany

[b] Instituto de Electroquímica, Universidad de Alicante, Apdo. 99, Alicante, Spain

[c] Helmholtz Institute Ulm (HIU) Electrochemical Energy Storage, 89069 Ulm, Germany

Abstract

Electrocatalytic activity is influenced by the surface charge on the solid catalyst. Conventionally, our attention has been focused on how the surface charge shapes the electric potential and concentration of ionic reactant(s) in the local reaction zone. Taking H_2O_2 redox reactions at Pt(111) as a model system, we reveal a peculiar surface charge effect using ab initio molecular dynamics simulations of electrified Pt(111)-water interfaces. In this scenario, the negative surface charge on Pt(111) repels the O-O bond of the reactant (H_2O_2) farther away from the electrode surface. This leads to a higher activation barrier for breaking the O-O bond. Incorporating this microscopic mechanism into a microkinetic-double-layer model, we are able to semi-quantitatively interpret the pH-dependent activity of H_2O_2 redox reactions at Pt(111), especially the anomalously suppressed activity of H_2O_2 reduction with decreasing electrode potential. The relevance of the present surface charge effect is also examined in wider scenarios with different electrolyte cations, solution pHs, crystal facets of the catalyst, and model parameters. In contrast with previous mechanisms focusing on how surface charge influences the local reaction condition at a fixed reaction plane, the present work gives an example in which the location of the reaction plane is adjusted by the surface charge.

Introduction

The catalytic activity of many electrocatalytic reactions has been found to vary with the solution pH, and electrolyte cations that were previously regarded as spectators.[1-5] Mechanistic investigations into such electrolyte effects in electrocatalysis underline the need for a better understanding of the nanoscale interfacial region between the solid catalyst and the electrolyte solution, termed the electrochemical double layer (EDL).[6, 7]

The EDL structure and the distribution of ion concentrations and electric potential in the EDL are determined largely by electrostatic interactions modulated by the excess charge on the electrode surface (surface charge for short).[8, 9] Conventional understandings of surface charge effects in electrochemistry forms the basis for interpreting multifaceted electrolyte effects in electrocatalysis. Frumkin connected electrode kinetics and the EDL structure, leading to a corrected Butler - Volmer - Erdey-Grúz equation.[10] For the case of a single-electron electrode reaction, $\mathrm{R} \leftrightharpoons \mathrm{O} + \mathrm{e}$, it reads,

$$i_{\mathrm{ct}} = k_{\mathrm{R}} c_{\mathrm{R}}^{\mathrm{rp}} \exp\left(\frac{\alpha F}{RT}\eta\right) - k_{\mathrm{O}} c_{\mathrm{O}}^{\mathrm{rp}} \exp\left(-\frac{(1-\alpha)F}{RT}\eta\right) \quad (1)$$

where k_{R} and k_{O} are the rate constants, $c_{\mathrm{R}}^{\mathrm{rp}}$ and $c_{\mathrm{O}}^{\mathrm{rp}}$ are the concentrations at the reaction plane (rp) in the vicinity of the electrode surface, which are usually different from their counterparts in the bulk solution, $c_{\mathrm{R}}^{\mathrm{bulk}}$ and $c_{\mathrm{O}}^{\mathrm{bulk}}$, α is the transfer coefficient, and $\eta = E_{\mathrm{M}} - \phi_{\mathrm{S}}^{\mathrm{rp}} - E^{\ominus}$ is the overpotential with E_{M} being the electrode potential, $\phi_{\mathrm{S}}^{\mathrm{rp}}$ the electric potential at the reaction plane, and $E^{\ominus}$ the standard equilibrium potential. The local reaction conditions, $c_{\mathrm{R}}^{\mathrm{rp}}$, $c_{\mathrm{O}}^{\mathrm{rp}}$ and $\phi_{\mathrm{S}}^{\mathrm{rp}}$, can be calculated from a proper model of the EDL, see a recent tutorial.[11]

Surface charge effects on the local potential and ion concentration at the reaction plane are denoted Frumkin surface charge effects, or simply Frumkin effects, which have been well established for anionic

electroreduction on mercury and mercury-like electrodes.[12] The advent of flame annealing method opens up an avenue to study Frumkin effects on electrocatalytic reactions at single-crystal transition metals.[13-16] Electroreduction of $S_2O_8^{2-}$, a reaction of historical importance in understanding surface charge effects, was studied on (modified) single crystals of Ag in the 1980s,[17] Au in the 1990s,[18, 19], Bi in 2000,[20] and Pt more recently.[21, 22] Recent development leads to the use of $S_2O_8^{2-}$ as a probe of the surface charge on Pt single crystals, of which the aptness has been verified by the agreement with the results of the CO displacement method and the laser-induced temperature jump method.[22-24]

On the modelling side, Frumkin effects have been incorporated into microkinetic-double-layer models for a variety of electrocatalytic reactions, including oxygen reduction reaction (ORR),[25-27] oxygen evolution reaction (OER) and carbon dioxide reduction reaction among others.[4, 28] The neglect of Frumkin surface charge effects will underestimate the ORR overpotential by ~60 mV, according to a recent work.[27] Ringe et al. emphasized the importance of the interfacial electric field on the adsorption energy of reaction intermediates with an inherent dipole moment.[4, 28]

Complexities beyond the Frumkin effects arise when local solvent configurations are considered in the picture. On the continuum level, the local dielectric constant of the solvation medium is dependent on the local electric field and the solvent density, which are influenced by the surface charge density.[29-31] Therefore, the local solvent organization energy, a key quantity in electron transfer theory, is dependent on the surface charge density, and eventually on the electrode potential, see Figure 5b in Ref.[29]. On the atomistic level, there is a paucity of understanding on how the local reaction environment is shaped by the surface charge density. Only recently has ab initio molecular dynamics (AIMD) been applied to study the EDL at metal-water interfaces.[32-37] In AIMD simulations, the surface charge can be modulated by removing (adding) atoms from (into) water layers. The structural transitions of interfacial water at electrified metal surfaces, proposed earlier by Iwasita and Xia,[38] was confirmed recently by Li et al. using in situ Raman spectroscopy.[39]

The present work studies surface charge effects on the redox reactions of H_2O_2 at Pt(111). There have been continued research interest in the electrocatalysis of H_2O_2 [40-47], mainly because H_2O_2 is an important intermediate of the ORR.[48] The obtained understanding may help in reducing the high overpotential of ORR, the performance-limiting reaction of polymer electrolyte fuel cells. Though much effort has been made for this model reaction, the redox behaviors of H_2O_2, even at structurally well-defined singe crystals such as Pt(111), are not completely understood. Specifically, as to be argued in the next section, the origins of the suppressed activity of H_2O_2 reduction with decreasing the electrode potential remain unclear.[45, 47] It is thus the main purpose of this work to advance the understanding of this model reaction.

The remainder of this paper is organized as follows. In section two, we introduce anomalous pH-dependent catalytic activity of H_2O_2 redox reactions at Pt(111) that has been observed frequently in experiments.[45, 47] In section three, we propose a mechanism for the suppressed activity of H_2O_2 reduction with decreasing the electrode potential, based on atomistic insights into how the EDL is shaped by the surface charge. In section four, we develop a microkinetic-double-layer model based on the obtained atomistic insights. In section five, we present a semi-quantitative model-based analysis of experimental data. In section six, we examine how variations in parameters of the model affect the results. In section seven, we further examine the present model in broader scenarios, including different cations, a wider pH range, and stepped Pt single crystals. Finally, we put the surface charge effect presented herein in a wider picture including various surface charge effects in electrocatalysis.

pH-dependent catalytic activity and its correlation with the surface charge

Figure 1 (a) displays the polarization curves of hydrogen peroxide reduction and oxidation reaction (HPRR/HPOR) at Pt(111) for five pHs, which have been reported by some of us previously.[47] The solution pH is tuned by mixing 0.1 M NaF and $\left(0.1+10^{-\mathrm{pH}}+\mathrm{K_{HF}}\right)/\left(1+\mathrm{K_{HF}}10^{\mathrm{pH}}\right)$ M $HClO_4$ with $K_{\mathrm{HF}}=7.2\times 10^{-4}$ being the dissociation constant of HF, see the calculation in the subsection of model parameters. The

concentration of H_2O_2 is 1.7 mM. The apparent current density $\tilde{J}_{app}$ is normalized with respect to the diffusional limiting current density.

The polarization curves are divided into four regions. In the region 1, $\tilde{J}_{app}$ decreases at higher pHs. In the region 2, $\tilde{J}_{app}$ is almost independent on the solution pH. In the region 3, $\tilde{J}_{app}$ is suppressed with decreasing the electrode potential, and the suppression occurs at higher potentials for higher pHs. In the region 4, the polarization curves converge more or less into a single curve.

Most previous discussion was centered around the suppression of HPRR in the region 3, while the other three regions are less discussed.[41, 44, 45, 47] Briega-Martos et al. attributed the suppression of HPRR to the negative surface charge density on the surface of Pt(111), rather than the site blocking effect of adsorbed hydrogen, because the suppression also occurs in the pure double layer charging region without any adsorbed hydrogen for pH=3.0, 4.0, 5.4.[45, 47]

To corroborate this surface charge effect, Figure 1(b) shows the magnitude of the intrinsic kinetic current density of HPRR $|\tilde{J}_{int}|$ versus the surface charge density σ_M in the region 3. $|\tilde{J}_{int}|$ is calculated from $\tilde{J}_{app}$ using $|\tilde{J}_{int}| = -\left(1 + \frac{1}{\tilde{J}_{app}}\right)^{-1}$ based on the dimensionless Koutecky-Levich equation, and σ_M is estimated from

$$\sigma_M = C_{dl}\left(E_{M,SHE} - E_{pzc,SHE}\right), \quad (2)$$

where C_{dl} is the double-layer capacitance, $E_{M,SHE}$ is the electrode potential on the SHE scale, and $E_{pzc,SHE}$ is the potential of zero charge (pzc) on the SHE scale. In this preliminary analysis, we assume $C_{dl} = 0.3\ \mathrm{F\ m^{-2}}$,[49, 50] and $E_{pzc,SHE} = 0.30\ \mathrm{V_{SHE}}$.[51] A more accurate analysis needs to consider the potential dependence of C_{dl}, which will be treated in a comprehensive model.

Figure 1 (b) shows that $|\tilde{J}_{int}|$ is positively correlated with σ_M. Notably, the four curves at pH = 2.1, 3.0, 4.0

and 5.4 are approximately collapsed into a single trend, lending credence to the view that the suppression of HPRR in the region 3 is related to the negative surface charge density on Pt(111).[45, 47]

However, the microscopic origin of the surface charge effect remains unclear. On the one hand, the surface charge effect on the local concentration of H_2O_2 should be less marked as H_2O_2 is an electroneutral molecule. On the other hand, the surface charge effect on the local electric potential is also less relevant here because HPRR is limited by a chemical step ($H_2O_2 \rightarrow 2OH_{ad}$) in the region 3.[40] Briega-Martos et al. attributed the suppression of the HPRR to the change of interfacial water configuration from hydrogen-up to hydrogen-down, when the surface charge density turns from positive to negative.[47] However, it remains unclear why the HPRR is suppressed by interfacial water molecules in the hydrogen-down configuration.

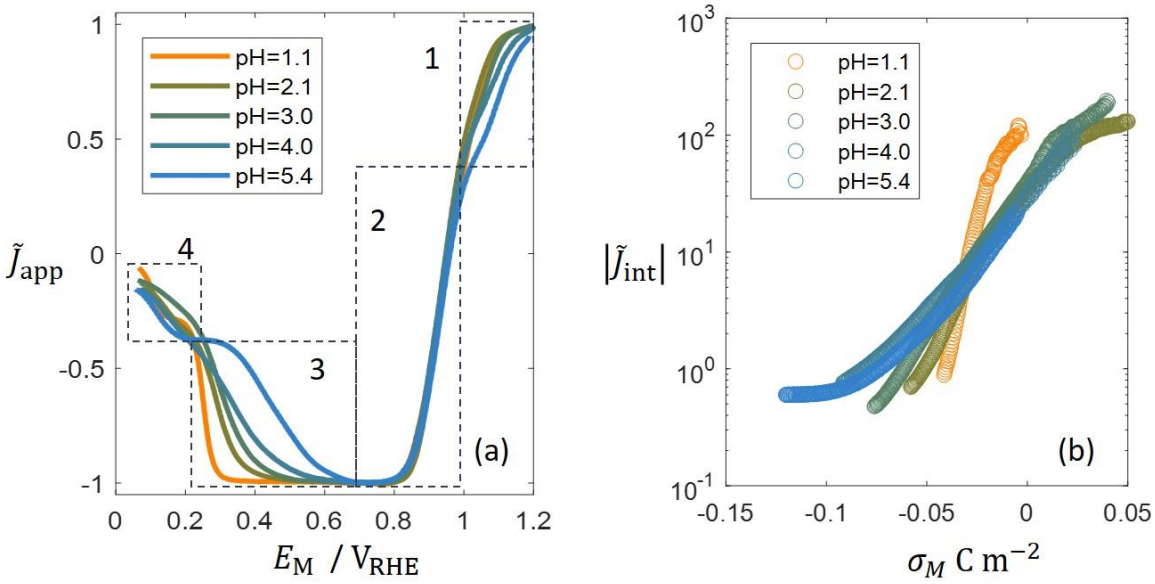

Fig. 1. (a) Polarization curves of hydrogen peroxide reduction and oxidation at Pt(111).[47] $\tilde{J}_{app}$ represents the dimensionless apparent current density normalized to the diffusional limiting current density. The electrolyte solution was prepared with NaF/$HClO_4$ mixtures and 1.7 mM H_2O_2. The scan rate is 50 $mV\ s^{-1}$ and the rotation rate is 2500 rpm. The polarization curves are divided into four regions with descriptions detailed in the main text. (b) The

absolute intrinsic kinetic current density ($|\tilde{\jmath}_{\mathrm{int}}|$) in the region 3 as a function of the surface charge density (σ_{M}) calculated from Eq.(2) with $C_{\mathrm{dl}} = 0.3\ \mathrm{F\ m^{-2}}$, and $E_{\mathrm{pzc,SHE}} = 0.30\ \mathrm{V_{SHE}}$.

A postulate of surface charge effect on HPRR based on AIMD simulations

To obtain atomistic insights into the surface charge effects, we employ AIMD simulations to simulate the interfacial structure of an electrified Pt(111) slab interfaced with an aqueous solution. The case of a positively charged Pt(111) slab is mimicked by adding a fluorine atom in water. The F atom will take one electron from Pt(111), resulting in a F^- anion in water and a positively charged Pt(111).[35-37] Similarly, we add a lithium atom in water to mimic a negatively charged Pt(111). An extra ion in solution corresponds to a surface charge density of ca. $\pm\ 0.146\ \mathrm{C\ m^{-2}}$ (+ for F^- and – for Li^+). A caveat is needed here. The definition of the surface charge becomes problematic in any atomistic picture of the EDL because there is no clear-cut allocation of metal electrons any longer in the presence of water molecules. We also add one H_2O_2 molecule to the water layer. More details of the AIMD simulation can be found in the SI.

Figure 2 (a) and (b) show snapshots of the negatively and positively charged Pt(111), respectively. Figure 2 (c) shows the variation of the total energy. The system is stabilized quickly after the first few hundreds of simulation steps, because the equilibrium structure of the water layer obtained in a previous work was inherited here as the initial configuration.[35] In line with previous works,[32, 34, 35, 39] on the positively charged surface, there is a larger surface coverage of water molecules bound strongly through their oxygen atom so that the hydrogen atoms of the water molecule are above the oxygen atoms. When the surface becomes negatively charged, the number of these strongly bound water molecules decreases which leads to a higher fraction of water molecules at the surface with their hydrogen atoms oriented towards the metal.[33, 37, 52]

The medium distance of the two oxygen atoms of H_2O_2 away from the outermost layer of Pt atoms is denoted $\bar{d}$. Figure 2 (d) shows the histograms of $\bar{d}$ over 4000 steps after the initial relaxation stage. We find that the O-O bond of the H_2O_2 molecule is farther away from the negatively charged Pt(111) compared to the positively charged case. Specifically, $\bar{d}$ is 2.98 Å for the positively charged case and 3.34 Å for the negatively charged case.

There are multiple factors contributing to a larger $\bar{d}$ for the negatively charged case. First, the negative surface charge repels via electrostatic forces negatively charged oxygen atoms of H_2O_2. Second, the H_2O_2 molecule is dragged away from the negatively charged electrode surface with the aid of the first water layer which is known to be farther away from a negatively charged electrode surface. Third, the nearby Li^+ ion with a full solvation shell pulls back H_2O_2 via a weak Li-O bond, see Figure 2 (a). The third factor may be invalid for other types of cations.

Since the electronic coupling exerted by the electrode decays exponentially with $\bar{d}$, *e.g.* Eq. 3 in ref.[53], the activation energy of breaking the O-O bond of H_2O_2 is expected to be higher for the negatively charged case with a higher $\bar{d}$. As HPRR is limited by the chemical step of breaking the O-O bond, this provides an appealing explanation for the suppressed activity of HPRR at the negatively charged Pt(111). We note that this explanation, albeit being seemingly reasonable, is still a postulate rather than a proof, since we have neither measured or calculated the activation energy of breaking the O-O bond. However, the aptness of this postulate is to be demonstrated below by comparing a microkinetic-double-layer model built upon this postulate and experimental data.

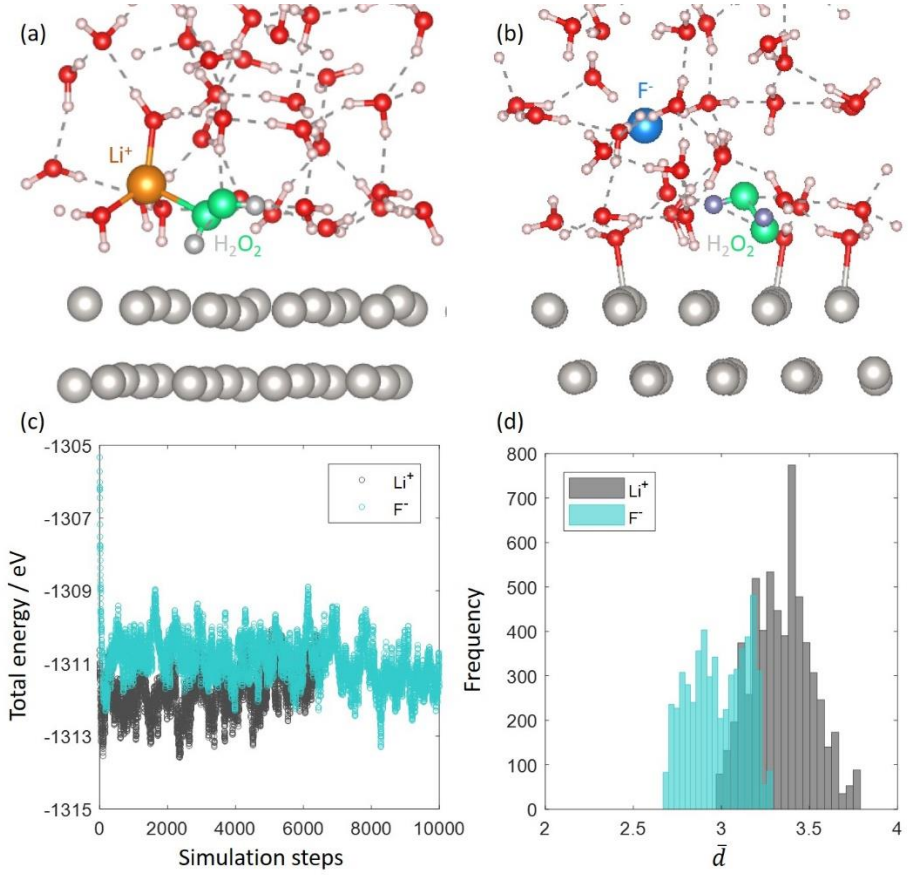

Fig. 2. Snapshots of the configuration of charged Pt(111) – water interfaces with one H_2O_2 molecule in water: (a) the negatively charged Pt(111) with one Li^+ cation in water; (b) the positively charged Pt(111) with one F^- anion in water. (c) Variation of the total energy with the simulation step for the two cases. (d) Histograms of the medium distance of the two oxygen atoms of the H_2O_2 molecule away from the outermost layer of Pt atoms.

A microkinetic-double-layer model

Built on the atomistic insights obtained from AIMD simulations, we proceed to semi-quantitatively analyze the polarization curves displayed in Figure 1 (a). This requires a physicochemical model for HPRR/HPOR, consisting of a microkinetic submodel describing multistep reaction kinetics and an EDL submodel describing local reaction conditions. Such a microkinetic-double-layer model, also termed a two-scale model by Bruix et al.,[54] is developed in this section with Matlab scripts enclosed the SI.

Reaction mechanism

We consider the following reaction mechanism for HPRR,

$$H_2O_2 + 2\blacksquare^{R} \leftrightarrow 2OH_{ad} \quad \text{(R1)}$$

$$H_2O + \blacksquare^{R} \leftrightarrow OH_{ad} + H^+ + e \quad \text{(R2)}$$

where $\blacksquare^{R}$ represent active sites for HPRR, and the following reaction mechanism for HPOR,

$$H_2O_2 + \blacksquare^{O} \leftrightarrow OOH_{ad} + H^+ + e \quad \text{(O1)}$$

$$OOH_{ad} \leftrightarrow O_2 + H^+ + e + \blacksquare^{O} \quad \text{(O2)}$$

where $\blacksquare^{O}$ represent active sites for HPOR. The dissociation-electrochemical mechanism of the HPRR expressed in Eq. (R1) and (R2) is widely held in the literature.[40, 47] However, different opinions exist for the HPOR in the presence of oxygenated species on Pt(111). Katsounaros et al. proposed a single chemical step: $2OH_{ad} + H_2O_2 \rightarrow 2H_2O + O_2$, coupled with formation of OH_{ad} from water dissociation.[40] OH_{ad} formation on Pt(111) is a quasi-equilibrium process that is pH-independent on the RHE scale in the acidic regime, as seen from cyclic voltammograms, e.g., in ref.[51]. Therefore, the region 1 where the HPOR dominates over the HPRR should be pH-independent on the RHE scale, according to the mechanism proposed by Katsounaros et al.[40] However, experimental data in Figure 1 (a) show that the region 1 is markedly pH dependent. Hence, the chemical step proposed by Katsounaros et al.[40] is not considered here. The preceding analysis does not defy the validity of the mechanism of Katsounaros et al. proposed for a polycrystalline Pt electrode whose electrochemistry is radically different from Pt(111) considered here.

We also consider hydrogen adsorption in the low potential region which competes for the adsorption sites,

$$H_{ad} \leftrightarrow \blacksquare^{S} + H^+ + e \quad \text{(S)}$$

Here, we have distinguished three types of adsorption sites, denoted with superscripts ‘R’ for HPRR, ‘O’ for HPOR, and ‘S’ for the side reaction hydrogen adsorption. The elementary steps are all written in a form with oxidation proceeding in the forward direction, so the HPRR proceeds in the forward direction of the step (R1) and then the backward direction of the step (R2). Different adsorption sites are assigned for reduction

and oxidation of hydrogen peroxide, otherwise the adsorption sites are completely occupied by OH_{ad} in high potential range and the HPOR cannot occur.

The reaction rates of the elementary steps of HPRR and HPOR are given by,

$$v_{\mathrm{R1}} = k_{\mathrm{R1}}^{+} c_{\mathrm{hp}} \left(\theta_{\mathrm{v}}^{\mathrm{R}}\right)^2 - k_{\mathrm{R1}}^{-} (\theta_{\mathrm{OH}})^2 \tag{3}$$

$$v_{\mathrm{R2}} = k_{\mathrm{R2}}^{+} \theta_{\mathrm{v}}^{\mathrm{R}} - k_{\mathrm{R2}}^{-} c_{\mathrm{p}}^{\mathrm{rp}} \theta_{\mathrm{OH}} \tag{4}$$

$$v_{\mathrm{O1}} = k_{\mathrm{O1}}^{+} c_{\mathrm{hp}} \theta_{\mathrm{v}}^{\mathrm{O}} - k_{\mathrm{O1}}^{-} c_{\mathrm{p}}^{\mathrm{rp}} \theta_{\mathrm{OOH}} \tag{5}$$

$$v_{\mathrm{O2}} = k_{\mathrm{O2}}^{+} \theta_{\mathrm{OOH}} \tag{6}$$

where $k_{\mathrm{i}}^{\pm}$'s represent the reaction rate constants (+ for oxidation, and – for reduction), c_{hp} the dimensionless concentration of hydrogen peroxide normalized to 1M, $c_{\mathrm{p}}^{\mathrm{rp}}$ the dimensionless local concentration of protons normalized to 1M at the reaction plane, $\theta_{\mathrm{v}}^{\mathrm{R/O}}$ the coverage of vacant adsorption sites of type 'R/O', θ_{OH} the coverage of adsorbed OH, the reaction intermediate of HPRR, θ_{OOH} the coverage of adsorbed OOH, the reaction intermediate of HPOR.

Under steady state condition, θ_{OH} and θ_{OOH} are time-invariant, leading to two equalities,

$$2v_{\mathrm{R1}} + v_{\mathrm{R2}} = 0 \tag{7}$$

$$v_{\mathrm{O1}} = v_{\mathrm{O2}} \tag{8}$$

The intrinsic kinetic current density is written as,

$$j_{\mathrm{int}} = \rho \mathrm{e}_0 (v_{\mathrm{O1}} + v_{\mathrm{O2}} + v_{\mathrm{R2}}) = \rho \mathrm{e}_0 (2v_{\mathrm{O1}} - 2v_{\mathrm{R1}}), \tag{9}$$

with ρ the number density of adsorption sites. The current density is positive for oxidation and negative for reduction. The apparent current density measured in rotating disk electrode experiments is influenced by mass transport effects,

$$\left(j_{\mathrm{app}}\right)^{-1} = (j_{\mathrm{int}})^{-1} + (j_{\mathrm{mtl}})^{-1} \tag{10}$$

where j_{mtl} is the mass-transport limiting current density given by the Levich equation[55],

$$j_{\mathrm{mtl}} = 0.643nFc_{\mathrm{hp}}D_{\mathrm{hp}}^{\frac{2}{3}}\nu^{-\frac{1}{6}}\omega^{\frac{1}{2}} \tag{11}$$

with $n = 2$ for HPOR and $n = -2$ for HPRR, D_{hp} the diffusion coefficient of hydrogen peroxide in aqueous solution, ν the viscosity of the electrolyte solution, and ω the rotating speed.

Hydrogen adsorption is so fast such that it is under quasi-equilibrium. Therefore, the coverage of $\mathrm{H_{ad}}$ can be found from the Frumkin adsorption isotherm,

$$\ln\left(\frac{\theta_{\mathrm{H}}}{1-\theta_{\mathrm{H}}}\right) + 2.3\mathrm{pH} + \frac{\chi_{\mathrm{H}}\theta_{\mathrm{H}} + \mathrm{e}_0E_{\mathrm{M}} - \Delta G(\mathrm{H})}{k_{\mathrm{B}}T} = 0 \tag{12}$$

where pH represents the pH in bulk solution, χ_{H} the lateral interaction coefficient, E_{M} the electrode potential on the SHE scale, $\Delta G(\mathrm{H})$ the adsorption energy of $\mathrm{H_{ad}}$ under the standard conditions.

The maximum coverage of adsorbed $\mathrm{OH_{ad}}$, $\theta_{\mathrm{OH}}^{\mathrm{max}}$, shall decrease in the presence of a large amount of $\mathrm{H_{ad}}$, described as,

$$\theta_{\mathrm{OH}}^{\mathrm{max}} = \min(\theta_{\mathrm{R}}^{\mathrm{max}}, 1-\theta_{\mathrm{H}}) \tag{13}$$

which means that the site-blocking effect of $\mathrm{H_{ad}}$ commences when $\theta_{\mathrm{H}} > 1-\theta_{\mathrm{R}}^{\mathrm{max}}$ with $\theta_{\mathrm{R}}^{\mathrm{max}}$ being the maximum fraction of adsorption sites for HPRR. We do not need to have a similar modification for the HPOR because hydrogen adsorption does not occur in the potential region of the HPOR.

The conservation of adsorption sites requires,

$$\theta_{\mathrm{OH}}^{\mathrm{max}} = \theta_{\mathrm{OH}} + \theta_{\mathrm{v}}^{\mathrm{R}} \tag{14}$$

for the HPRR. Similarly, we have,

$$\theta_{\mathrm{OOH}}^{\mathrm{max}} = \theta_{\mathrm{OOH}} + \theta_{\mathrm{v}}^{\mathrm{O}} \tag{15}$$

for the HPOR.

Rate constants

The rate constants of electrochemical steps, R2, O1, O2, are described using transition state theory,

$$k_{\mathrm{i}}^{\pm} = \frac{k_{\mathrm{B}}T}{h}\exp\left(-\frac{G_{a,i}^{0} \pm \beta_i^{\pm}\eta_i}{kT}\right) \tag{16}$$

where $G_{a,i}^{0}$ is the activation energy of step i ($i = \mathrm{R2}, \mathrm{O1}, \mathrm{O2}$) under standard equilibrium conditions, $\beta_i^{\pm}$ is the symmetry factor of step i in the oxidation (+) / reduction (-) directions, η_i is the overpotential, which is given by,

$$\eta_i = E_{\mathrm{M}} - \phi_{\mathrm{S}}^{\mathrm{rp}} - E_i^{\ominus} \tag{17}$$

with $\phi_{\mathrm{S}}^{\mathrm{rp}}$ the electric potential at the reaction plane, and $E_i^{\ominus}$ the standard equilibrium potentials, which are calculated as,

$$\mathrm{e}_0 E_{\mathrm{R2}}^{\ominus} = \Delta G(\mathrm{OH}) \tag{18}$$

$$\mathrm{e}_0 E_{\mathrm{O1}}^{\ominus} = \Delta G(\mathrm{OOH}) - \Delta G(\mathrm{H_2O_2}) \tag{19}$$

$$\mathrm{e}_0 E_{\mathrm{O2}}^{\ominus} = \Delta G(\mathrm{O_2}) - \Delta G(\mathrm{OOH}) \tag{20}$$

with $\Delta G(\mathrm{OH})$ and $\Delta G(\mathrm{OOH})$ the binding energies of $\mathrm{OH_{ad}}$ and $\mathrm{OOH_{ad}}$, $\Delta G(\mathrm{O_2}) = 4.92$ eV the Gibbs free energy of the reaction $2\mathrm{H_2O} \leftrightarrow \mathrm{O_2} + 2\mathrm{H_2}$ under standard equilibrium conditions, and $\Delta G(\mathrm{H_2O_2}) = 3.53$ eV the Gibbs free energy of the reaction $2\mathrm{H_2O} \leftrightarrow \mathrm{H_2O_2} + \mathrm{H_2}$ under standard equilibrium conditions. The binding energies of $\mathrm{OH_{ad}}$ and $\mathrm{OOH_{ad}}$ are defined as the Gibbs free energies of the reactions $\mathrm{H_2O} \leftrightarrow \mathrm{OH_{ad}} + \frac{1}{2}\mathrm{H_2}$, $2\mathrm{H_2O} \leftrightarrow \mathrm{OOH_{ad}} + \frac{3}{2}\mathrm{H_2}$, respectively, according to the computational hydrogen electrode approach.[56]

As for the chemical step R1, the forward reaction rate is described as,

$$k_{\mathrm{R1}}^{\pm} = \frac{k_{\mathrm{B}}T}{h}\exp\left(-\frac{G_{\mathrm{a,R1}} + \beta_{\mathrm{R1}}\Delta G_{\mathrm{R1}}}{kT}\right) \tag{21}$$

where $G_{\mathrm{a,R1}}$ is the activation energy under the standard equilibrium conditions, β_{R1} is the symmetry factor of this step, ΔG_{R1} is the Gibbs free energy,

$$\Delta G_{\mathrm{R1}} = 2\Delta\mathrm{G(OH)} - \Delta\mathrm{G}(\mathrm{H_2O_2}) \tag{22}$$

Considering surface charge effects on the location of the O-O bond of H_2O_2, $G_{\mathrm{a,R1}}$ should depend on σ_{M}. As a first approximation, we assume a linear relation with an upper bound,

$$G_{\mathrm{a,R1}} = \min\left(G_{\mathrm{a,R1}}^{0} + \chi\sigma_{\mathrm{M}}h(-\sigma_{\mathrm{M}}), G_{\mathrm{a,R1}}^{\max}\right) \tag{23}$$

where $G_{\mathrm{a,R1}}^{0}$ is the value of $G_{\mathrm{a,R1}}$ for the uncharged case, σ_{M} is the surface charge density, χ is the linear coefficient, $G_{\mathrm{a,R1}}^{\max}$ is the upper bound of $G_{\mathrm{a,R1}}$. $h(-\sigma_{\mathrm{M}}) = 1$ for $\sigma_{\mathrm{M}} < 0$ and $h(-\sigma_{\mathrm{M}}) = 0$ elsewise. Constraining $G_{\mathrm{a,R1}}$ in a feasible range is a simple remedy for the linear assumption between $G_{\mathrm{a,R1}}$ and σ_{M}.

Local reaction conditions

The local reaction conditions, including $\phi_{\mathrm{S}}^{\mathrm{rp}}$, $c_{\mathrm{p}}^{\mathrm{rp}}$, and σ_{M}, are calculated from an EDL model. The mean-field grand potential per unit volume of the electrolyte solution is written as,[57]

$$g = -\frac{1}{2}\epsilon_S E^2 + \sum_{l=1}^{\mathrm{N_{ion}}} n_l q_l \phi + \sum_{l=1}^{\mathrm{N_{ion}}} \beta^{-1} n_l\left(\ln\left(n_l\Lambda_l^3\right) - 1\right) + \Phi_{\mathrm{ex}}(\{n_l\}) - \sum_{l=1}^{\mathrm{N_{ion}}} n_l\tilde{\mu}_l \tag{24}$$

where ϵ_S is the dielectric constant of the electrolyte solution, ϕ the electric potential, $E = \nabla\phi$ the electrical field, $\mathrm{N_{ion}}$ number of types of ions, q_l charge number of ions of type l, n_l number density of ions of type l, $\beta = 1/k_{\mathrm{B}}T$ the inverse thermal energy, Λ_l thermal wavelength of ions of type l, which normalizes n_l, $\Phi_{\mathrm{ex}}(\{n_l\})$ excess free energy per unit volume that accounts for the deviation of the electrolyte solution from an ideal gas system, $\tilde{\mu}_l$ electrochemical potentials of ions of type l, which are bulk properties.

Use is then made of the variational principle, resulting in the following Euler-Lagrange equation in terms of ϕ,

$$\frac{\partial g}{\partial \phi} - \frac{\partial}{\partial x}\left(\frac{\partial g}{\partial E}\right) = 0. \tag{25}$$

Substituting Eq.(24) into Eq.(25), we obtain the Poisson-Boltzmann (PB) equation,

$$-\frac{\partial}{\partial x}\left(\epsilon_S \frac{\partial \phi}{\partial x}\right) = \sum_{l=1}^{\mathrm{N_{ion}}} n_l q_l. \tag{26}$$

In the same manner, we can write down the following Euler-Lagrange equation in terms of n_l,

$$\frac{\partial g}{\partial n_l} - \frac{\partial}{\partial x}\left(\frac{\partial g}{\partial(\nabla n_l)}\right) = 0, \tag{27}$$

leading to,

$$n_l = n_{\max} \frac{\chi_l \exp\left(-\beta q_l(\phi - \phi_{\mathrm{S}}^{\mathrm{b}})\right)}{1 + \sum_{l=1}^{N_{\mathrm{ion}}} \chi_l \left(\exp\left(-\beta q_l(\phi - \phi_{\mathrm{S}}^{\mathrm{b}})\right) - 1\right)} \tag{28}$$

with $\chi_l = n_l^{\mathrm{b}}/n_{\max}$ the dimensionless number density of ions of type l, $n_{\max}$ the maximum number density, n_l^{b} the number density of ions of type l in the bulk solution, $\phi_{\mathrm{S}}^{\mathrm{b}}$ the potential in the bulk solution.

Here, we have used the Bikerman theory for $\Phi_{\mathrm{ex}}(\{n_l\})$, which gives,[57]

$$\mu_l^{\mathrm{ex}} = \beta^{-1}\frac{\delta \Phi_{\mathrm{ex}}}{\delta n_i} = \beta^{-1}\ln\left(\frac{n_{\max}}{n_{\max} - \sum_{l=1}^{N_{\mathrm{ion}}} n_l}\right) \tag{29}$$

Substituting Eq. (28) into Eq.(26) leads to a single second-order differential equation in terms of ϕ. Boundary conditions to close Eq.(26) are as follows,

$$\phi = \phi_{\mathrm{S}}^{\mathrm{b}} = 0, \tag{30}$$

in the bulk solution, and

$$\phi = E_{\mathrm{M}} - E_{\mathrm{pzc}} + \delta_{\mathrm{rp}}\frac{\epsilon_{\mathrm{S}}}{\epsilon_{\mathrm{rp}}}\frac{\partial \phi}{\partial x}\Big|_{x=0} + \frac{\mu_{\mathrm{chem}}}{\epsilon_{\mathrm{rp}}}, \tag{31}$$

at the reaction plane, which is designated as the coordinate origin, $x = 0$. The space between the metal surface and the reaction plane has a thickness of δ_{rp} and a permittivity of ϵ_{rp}. E_{pzc} is the potential of zero charge of the electrode. The third term represents the potential change from the metal surface to the reaction plane caused by the excess free charge. The last term describes the potential drop caused by chemisorption-induced surface dipoles, μ_{chem}.[58] Based on the assumption that chemisorbates line up co-planarly and rigidly at the reaction plane, we calculate μ_{chem} as,

$$\mu_{\mathrm{chem}} = \sum_i \theta_i \gamma_i \delta_{\mathrm{ap}} \rho, \tag{32}$$

with γ_i the net charge number of chemisorbates of type *I*, and δ_{ap} the distance between the metal surface and the adsorbate plane. Note in passing that we have distinguished the reaction plane and the adsorbate plane, and δ_{ap} is generally smaller than δ_{rp}.

Model parameters and numerical implementation

The model, as summarized in Figure 3, is solved in Matlab with the scripts provided in the SI. The controlling equation for the electric potential, Eq.(26), is solved using the built-in function 'bvp4c' in Matlab. The boundary condition at the reaction plane, Eq.(31), needs coverages of chemisorbates that are found from nonlinear equations, Eqs.(7)(8), of the microkinetic model. The microkinetic model is coded as a function termed 'SurfR' which determines θ_{OH} and θ_{OOH} as a function of any local potential and electric field.

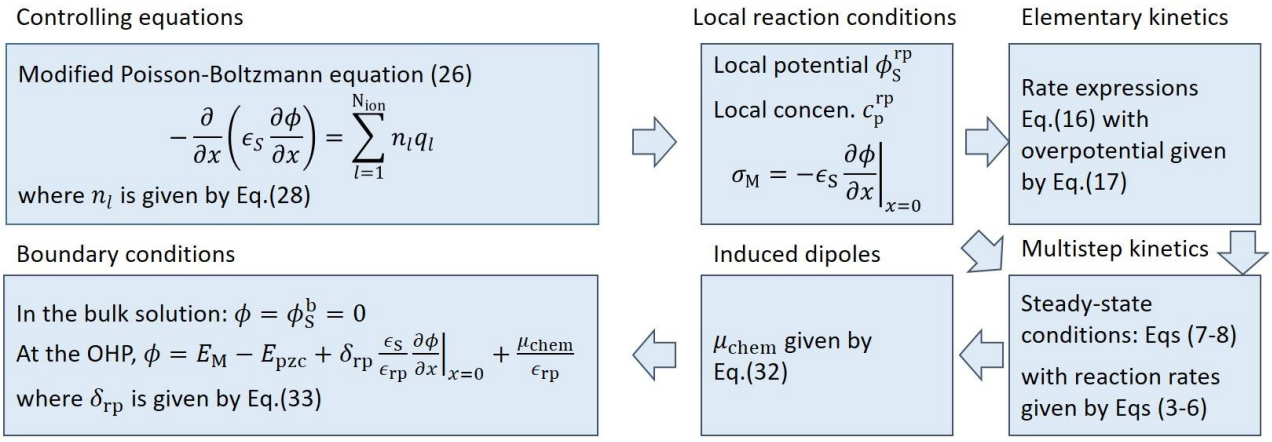

Fig. 3. Flowchart of solving the microkinetic-double-layer model.

Model parameters are divided into four categories: electrode, electrolyte solution, EDL structure and reactions. A basic set of model parameters are obtained by fitting the model with the polarization curve of the HPRR and HPOR at Pt(111) in an electrolyte solution a pH of 2. Model parameters are tuned by hand. In the following, we explain the parameters, either calculated or adopted or fitted.

1) Electrode

Pt(111) is employed as the electrode. The areal number density of Pt atoms is calculated as, $\rho = \frac{4}{\sqrt{3}a_{\mathrm{Pt111}}^2} = 1.5 \times 10^{15}\ \mathrm{m}^{-2}$, using the lattice constant of Pt(111) $a_{\mathrm{Pt111}} = 3.92\ \text{Å}$. The potential of zero charge is 0.30 V vs the standard hydrogen electrode (SHE), as measured by the CO displacement method and the laser-induced temperature jump method.[14, 51]

2) Electrolyte solution

The electrolyte solution is composed of 0.1 M NaF, x M $HClO_4$ and 1.7 mM H_2O_2, according to the experimental study.[47] The solution pH is tuned by mixing NaF and HClO4. The concentration of NaF is calculated from, $\mathrm{K_{HF}} = \frac{[\mathrm{H^+}][\mathrm{F^-}]}{[\mathrm{HF}]} = \frac{10^{-\mathrm{pH}}\left(0.1+10^{-\mathrm{pH}}-x\right)}{\left(x-10^{-\mathrm{pH}}\right)}$, where $\mathrm{K_{HF}} = 7.2 \times 10^{-4}$ is the dissociation constant of HF (pKa=3.14).[59] We obtain $x = \frac{0.1+10^{-\mathrm{pH}}+\mathrm{K_{HF}}}{1+\mathrm{K_{HF}}10^{\mathrm{pH}}}$.

Therefore, the electrolyte cations include 0.1 M Na^+ and $10^{-\mathrm{pH}}$ M H^+, the electrolyte anions include x M $\mathrm{ClO_4^-}$ and $\left(0.1 + 10^{-\mathrm{pH}} - x\right)$ M $\mathrm{F^-}$. The maximum number density $\mathrm{n_{max}}$ is calculated as the sum of number densities of all particles in the bulk solution. Therefore, the dimensionless number densities of ions in the bulk solution are calculated using $\chi_l = c_l^{\mathrm{b}} N_{\mathrm{A}}/n_{\mathrm{max}}$ with c_l^{b} the bulk concentration and N_{A} the Avogadro constant. The dielectric constant of the bulk solution is $78.5\epsilon_0$. The diffusion coefficient of hydrogen peroxide is $D_{\mathrm{hp}} = 2 \times 10^{-9}\ \mathrm{m^2 s^{-1}}$.[60] The viscosity of the electrolyte solution is $\nu = 8.91 \times 10^{-7}\ \mathrm{Pa \cdot s}$.

3) EDL structure

The space between the metal surface and the adsorbate plane has a fixed thickness of $\delta_{\mathrm{ap}} = 2\ \text{Å}$, while that between the metal surface and the reaction plane, which is designated as the medium plane of the O-O bond of the H_2O_2 molecule, δ_{rp} depends on σ_{M}. As a first approximation, we use a linear relation between δ_{rp} and σ_{M},

$$\delta_{\mathrm{rp}} = \delta_{\mathrm{rp}}^0 + \chi_{\mathrm{rp}}\sigma_{\mathrm{M}}, \tag{33}$$

where δ_{rp}^{0} is the value at an uncharged surface, and χ_{rp} is the linear coefficient which is negative, in accordance with the trend that δ_{rp} is larger at a negatively charged surface. We used $\delta_{\mathrm{rp}}^{0} = 3\ \text{Å}$ and $\chi_{\mathrm{rp}} = -5 \times 10^{-10}\mathrm{m^3C^{-1}}$. The permittivity of the space between the metal and the reaction plane is $\epsilon_{\mathrm{rp}} = 6\epsilon_0$, which is commonly used for the inner region of EDL.[61]

4) Reactions

We use $\Delta G(\mathrm{H}) = 0.30$ eV, $\Delta G(\mathrm{OH}) = 0.80$ eV and $\Delta G(\mathrm{OOH}) = 4.02$ eV for the binding energies of $\mathrm{OH_{ad}}$ and $\mathrm{OOH_{ad}}$, according to DFT calculations,[62] $\Delta G(\mathrm{O_2}) = 4.92$ eV for the Gibbs free energy of the reaction $2\mathrm{H_2O} \leftrightarrow \mathrm{O_2} + 2\mathrm{H_2}$ under the standard conditions, and $\Delta G(\mathrm{H_2O_2}) = 3.53$ eV for the Gibbs free energy of the reaction $2\mathrm{H_2O} \leftrightarrow \mathrm{H_2O_2} + \mathrm{H_2}$ under the standard conditions. The activation energies of elementary steps are tuned by hand, $G_{\mathrm{a,R2}}^{0} = 0.40$ eV, $G_{\mathrm{a,O1}}^{0} = 0.66$ eV, $G_{\mathrm{a,O2}}^{0} = 0.54$ eV. The symmetry factors are $\beta_i^{\pm} = 0.5$ for all electron transfer steps. The small magnitude of $G_{\mathrm{a,R2}}^{0}$ is in accord with the highly symmetric butterfly corresponding to adsorption/desorption of OH_{ad} in the cyclic voltammogram of Pt(111). The activation energy for step R1 under equilibrium is $G_{\mathrm{a,R1}}^{0} = 1.30$ eV (note that ΔG_{R1} is very negative, so $G_{\mathrm{a,R1}}$ is less than 0.5 eV). The coefficient reflecting the effect of surface charge on bond breaking is fitted as $\chi = -5.5$. The upper bound of $G_{a,R1}$ is set as $G_{\mathrm{a,R1}}^{\max} = 0.49$ eV. The maximum fractions of adsorption sites for HPRR and HPOR are assumed as $\theta_{\mathrm{R}}^{\max} = \theta_{\mathrm{OOH}}^{\max} = 1/3$.

Model-based analysis of pH-dependent catalytic activity of HPRR/HPOR

Model-based and experimental data are compared in Figure 4(a), for the base case of hydrogen peroxide reactions on Pt(111) in 0.1 M $HClO_4$, 0.1033 M NaF, and 1.7 mM H_2O_2 (pH = 2). Model parameters for this base case are provided in the SI. The parameterized model is then employed to simulate the polarization curves for other pHs. The corresponding experimental data are displayed in Figure 1 (a). Results for the case with $\chi = 0$, namely, without surface charge effects on the O-O bond breaking, are shown in Figure 4(b).

Overall, major experimental phenomena are captured by the model, including lower oxidation current at higher pHs in the region 1, weakly pH-dependent current in the region 2, earlier suppression of HPRR at

higher pHs in the region 3, and merging of different curves in the region 4. However, the suppression of HPRR is absent for case with $\chi = 0$, even though the traditional Frumkin effects on the local reaction conditions are included. Mechanistic understandings of these phenomena gleaned from the model are presented below, following the sequence of the regions 3, 4, 1, 2.

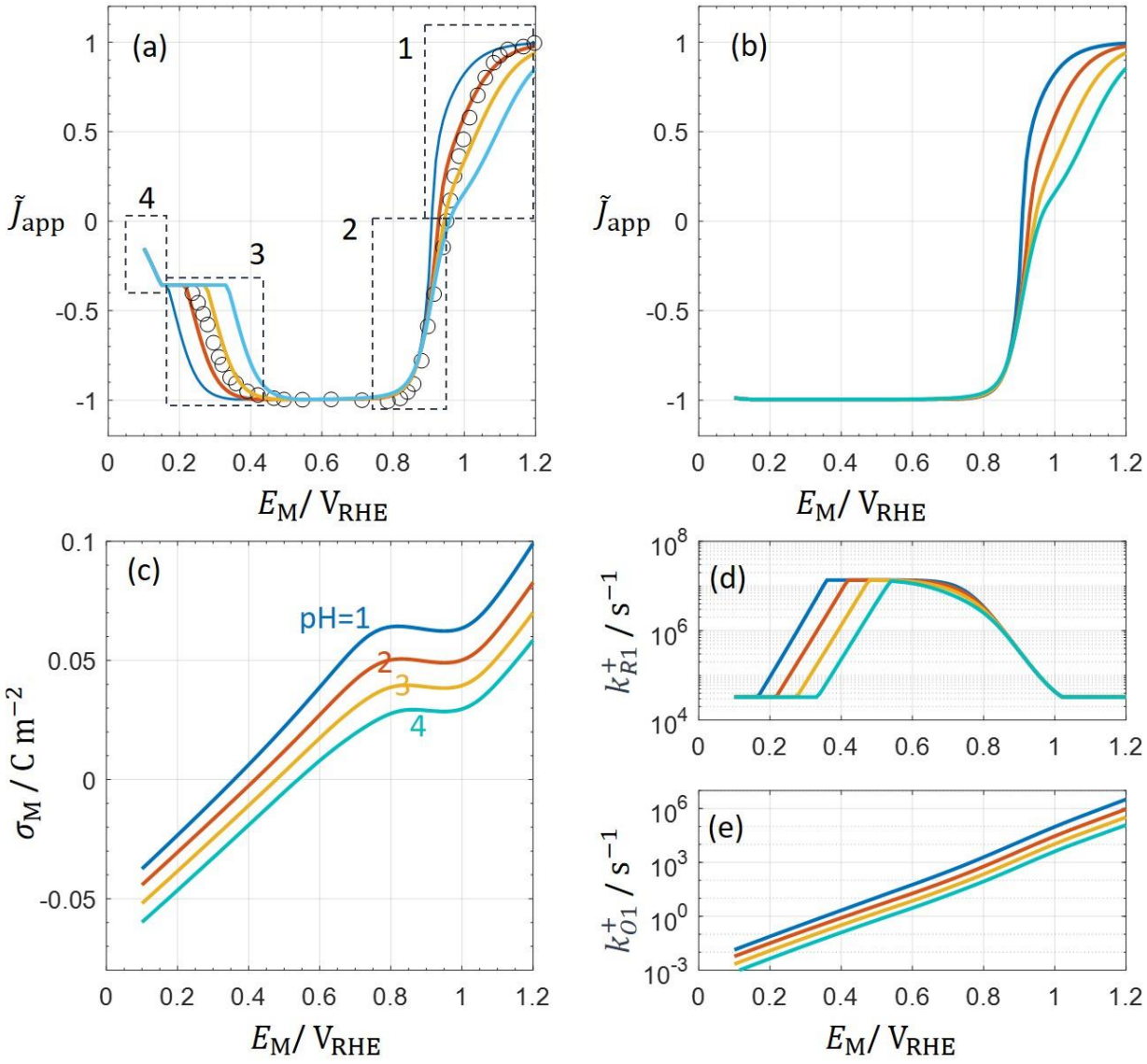

Fig. 4. Model-based analysis of hydrogen peroxide reactions at Pt(111). (a) Model-based polarization curves at four pHs, see legends in (c), and the experimental polarization curve for pH = 2, marked as circles. (b) Model-based polarization curves for the case of $\chi = 0$. (c) Surface charging behaviors at four pHs. (d) The forward reaction

constant of the step $\mathbf{H_2O_2 + 2{\blacksquare}^R \leftrightarrow 2OH_{ad}^R}$ at four pHs. (e) The forward reaction constant of the step $\mathbf{H_2O_2 + {\blacksquare}^O \leftrightarrow OOH_{ad}^O + H^+ + e}$ at four pHs.

In the region 3, the suppression of HPRR is caused by the negative surface charge on Pt(111), which repels the O-O bond of H_2O_2 farther away the electrode surface, as revealed by the AIMD simulations presented in Figure 2. Figure 4 (c) shows the surface charge density as a function of E_{M} on the RHE scale for four pHs. The surface charging curve shifts left, namely, σ_{M} becomes more negative at a given E_{M} versus the RHE, with increasing pH. This shift is an immediate consequence of the shift in the potential of zero charge (pzc) on the RHE scale with solution pH, expressed as, $E_{\mathrm{pzc}}^0 + 0.059 \cdot \mathrm{pH\ (V)}$ with E_{pzc}^0 being the pzc on the SHE scale. The nonmonotonic behavior of σ_{M} is due to the chemisorption of OH_{ad}, which introduces an additional potential drop at the interface, and effectively increases the pzc, as explained in previous works.[58, 63]

The activation barrier of breaking the O-O bond of $\mathrm{H_2O_2}$, denoted $G_{\mathrm{a,R1}}$ becomes higher when Pt(111) is more negatively charged. Figure 4 (d) shows the rate constant of this step, denoted k_{R1}^+, as a function of E_{M} on the RHE scale for four pHs. Following the surface charging relation in Figure 4 (c), k_{R1}^+ decreases exponentially (the y-axis is on the logarithm scale) with E_{M} in the region 3 and the curves shift to the right with increasing pH. There exists a plateau below 0.3 V_{RHE} because we have set an upper limit for $G_{\mathrm{a,R1}}$ in the model.

In the region 4, the merging of different curves is due to combined influence of two factors. On the one hand, $G_{\mathrm{a,R1}}$ reaches its upper limit so that k_{R1}^+ reaches its lower bound, see Figure 4 (d). On the other hand, the coverage of adsorbed hydrogen increases with lowering E_{M}, as shown in Figure S1 of the SI, decreasing the active sites for HPRR and impairing the activity of HPRR. Massive adsorbed H may exert repulsion on OH adsorption, which is, however, not considered in this model. Note in passing that the step-wise transition from the region 3 to 4 is just an artifact of the model.

In the region 1, the net oxidation current decreases at higher pHs. Let us consider the forward reaction rate of the step ($\mathrm{H_2O_2} + \blacksquare^{\mathrm{O}} \leftrightarrow \mathrm{OOH_{ad}} + \mathrm{H^+} + \mathrm{e}$), denoted k_{O1}^{+}. At a certain E_{M} on the RHE scale, the electrochemical potential of the electron is higher for a higher pH because of a lower E_{M} on the SHE scale. Therefore, k_{O1}^{+} becomes slower for higher pHs at a certain E_{M} on the RHE scale, as shown in Figure 4 (e), resulting in a lower net oxidation current at higher pHs. Under equilibrium, both elementary steps of HPOR, being proton-coupled electron transfer steps, should be pH-independent on the RHE scale. The pH-dependence observed in Figure 4 (b) is a manifestation of nonequilibrium microkinetics.

In the region 2, the pH-dependence is much weaker compared to that in the region 3. As shown in Figure S2, the HPRR is limited by the first step of O-O bond breaking. Inconsistent with the increasing σ_{M} above 0.8 V_{RHE} in Figure 4(c), k_{R1}^{+} decreases, see Figure 4(d). This is caused by lateral repulsion among OH_{ad}, resulting in a more positive ΔG_{OH} and a higher ΔG_1. As adsorption of OH is in thermodynamic equilibrium and in the absence of other species is pH-independent on the RHE scale, k_{R1}^{+} becomes pH-independent, so does the net reduction current density.

Parametric analysis of the model

We now discuss the influence of variations in model parameters on the model-based results. In the region 3, the model-based polarization curve is markedly affected by χ, see Figure 4(a) and (b), and EDL parameters determining σ_{M}. In Figure 5 (a), we evaluate two EDL parameters, δ_{rp}^{0} and ϵ_{rp}. A larger δ_{rp}^{0} leads to σ_{M} with a smaller magnitude at a particular potential, thus alleviating the suppression of HPRR in the region 3, see Figure 5(a). The same trend can be obtained by lowering ϵ_{rp}.

In the region 1, the observed current density is the sum of the HPRR and the HPOR. Therefore, the model-based polarization curve is sensitive to variations in the reaction parameters of elementary steps. For the basic set of model parameters, both the HPRR and the HPOR are limited by their first steps. Hence, the results are most sensitive to the parameters of these two steps. In Figure 5 (c), we show that a smaller (higher) $G_{\mathrm{a,O1}}^{0}$ shifts the polarization curve to the left (right) side.

The EDL model features a tunable reaction plane, introducing a coefficient χ_{rp} to describe the trend that the reaction plan is pushed away from the negatively charged metal surface, as expressed in Eq.(33). In Figure 5(d), we compare the EDL model with a negative χ_{rp} and that with a zero χ_{rp}, namely, a fixed reaction plane. It is found that σ_{M} decreases in the magnitude due to a negative χ_{rp} which increases the Stern layer when $\sigma_{\mathrm{M}} < 0$. The opposite is observed for $\sigma_{\mathrm{M}} > 0$.

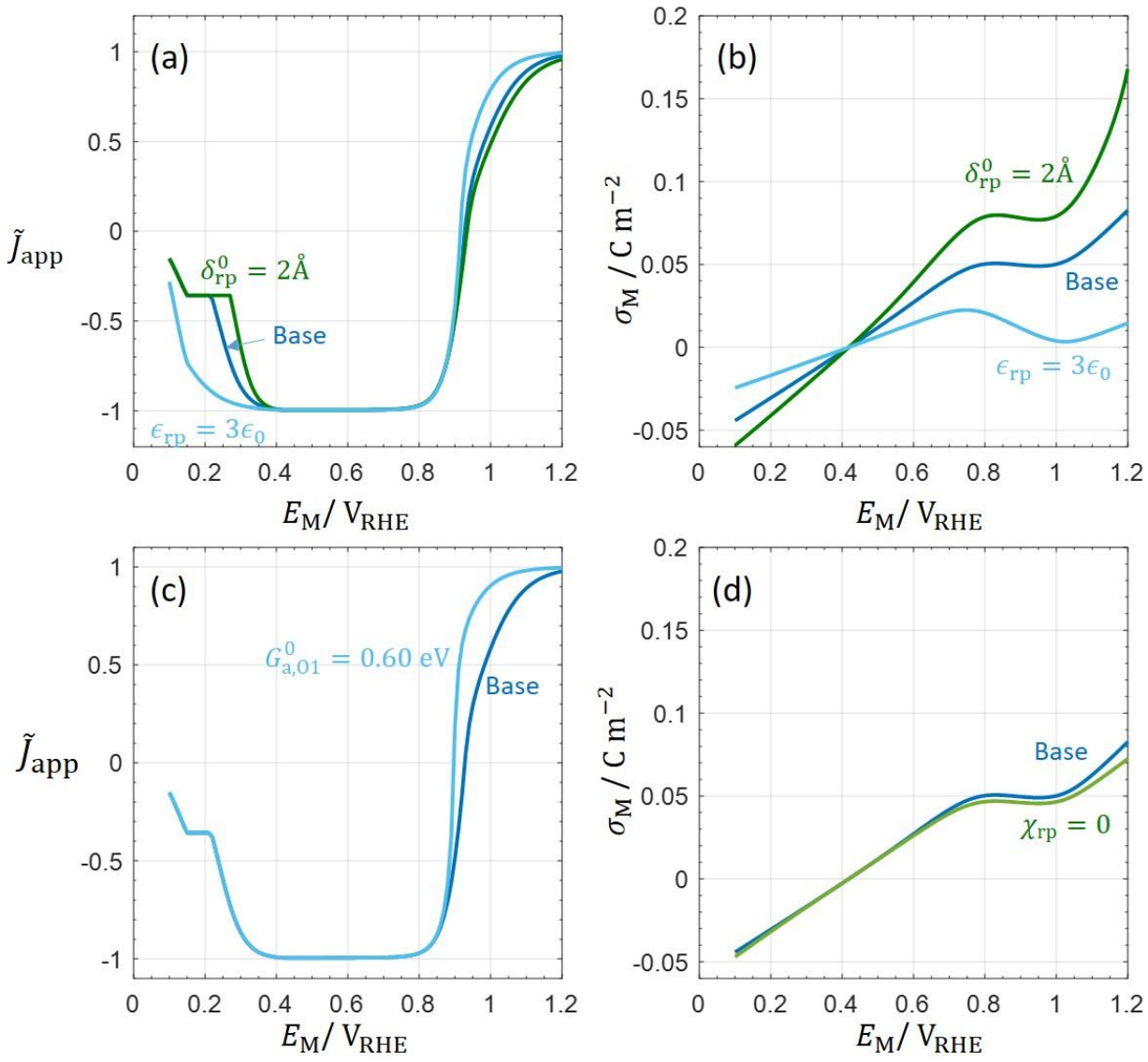

Fig. 5. Parametric analysis of the present model of hydrogen peroxide reactions at Pt(111). (a) Influence of EDL parameters on model-based polarization curves at pH = 2. The base line corresponds to the set of model parameters used in Fig.4, namely, $\boldsymbol{\delta_{\mathrm{rp}}^{0} = 3\ \text{Å}, \epsilon_{\mathrm{rp}} = 6\epsilon_0, \chi_{\mathrm{rp}} = -5 \times 10^{-10}\ \mathrm{m^3 C^{-1}}, G_{\mathrm{a,O1}}^{0} = 0.66\ \mathrm{eV}}$. Other lines are obtained

by varying a parameter with the modified value marked aside. (b) Influence of EDL parameters on surface charging relation at pH = 2. (c) Influence of $G^0_{a,O1}$ on model-based polarization curves at pH = 2. (d) Influence of χ_{rp} on the surface charging relation.

We have assumed symmetry factors $\beta_i^{\pm} = 0.5$ in above analysis. We know from fundamental theories of electrochemical electron transfer that $\beta_i^{\pm}$ shall vary with the electrode potential, see, e.g., ref.[64]. To examine the influence of potential-dependent $\beta_i^{\pm}$, we allow $\beta_i^{\pm}$ of electrochemical steps to vary randomly between 0.3 and 0.7 in Monte-Carlo simulations of the model. The results are shown in Figure S3. It is found that $\beta_i^{\pm}$ mainly changes the HPOR region (region 1 in Figure 4). The reason is that the HPRR is determined by the chemical step (R1), while the HPOR is determined by both electrochemical steps (O1 and O2).

Relevance of the surface charge effect in wider scenarios

The EDL properties can be tuned by changing the identity of cations. The resultant cation effects have been studied, both experimentally and theoretically, for various electrocatalytic reactions, see e.g., refs.[1-4]. For our case of hydrogen peroxide reactions, the cation effects can be studied by using different salts (LiF, NaF and CsF) to modulate the solution pH.[65] It is well known that Li^+ ions are "structural makers" and retain its complete solvation shell near the metal surface, as shown in Figure 2 (a).[66] On the contrary, Cs^+ are structural breakers and lose part of its solvation shell near the metal surface, as schematically shown in Figure 5 (a). In our model, the difference in the interfacial water structure surrounding cations can be reflected with different values of δ^0_{rp}. Given that Cs^+ can approach closer to the metal surface by partially taking off the solvation shell, a smaller δ^0_{rp} is assigned for Cs^+. A similar consideration has been taken by Ringe et al. when modelling the cation effects on CO2 reduction.[4, 28] A smaller δ^0_{rp} leads to a higher double layer capacitance. Correspondingly, the surface charging relation has a larger slope for the case of Cs^+ with a smaller δ_{rp}, as shown in Figure 5 (b). As σ_M is more negative for Cs^+ in the region 3, the O-O bond of H_2O_2 is repelled farther away from Pt(111) and $G_{a,R1}$ is higher, resulting in more significant suppression

of HPRR, as shown in Figure 5 (a). This trend has been observed in our recent experiments published elsewhere.[65] This cation effect further confirms the aptness of the present model.

So far, our analysis has been limited to the acidic regime and we now discuss it in the alkaline regime. The pzc on the RHE scale, calculated as $E^0_{\mathrm{pzc}} + 0.059 \cdot \mathrm{pH}\ (\mathrm{V})$, can be up to 0.9 V_{RHE} for pH>11. Following our previous line of reasoning, it is expected that the HPRR is suppressed below 0.9 V_{RHE} for pH>11. At odds with this reasoning, the suppression of HPRR occurs only below 0.6 V_{RHE} in 0.1 M NaOH, as shown in a recent experimental study.[44] This discrepancy indicates that either the surface charge effect is subordinate in the alkaline regime, or E^0_{pzc} has a different value in the alkaline regime. Laser-induced temperature jump is a surface-sensitive, in-situ method to probe E^0_{pzc}. Using this method, Sarabia et al. reported recently that E^0_{pzc} decreases from 0.30 V_{SHE} at pH=1 to -0.075 V_{SHE} at pH=13.[67] The origin of a pH-dependent E^0_{pzc} is of vital importance for interfacial electrochemistry, which is beyond the scope of this work.

Briega-Martos et al. reported that the suppression of HPRR in the region 3 is alleviated gradually with increasing the number density of (110) steps.[45] This phenomenon can be explained based on the Smoluchowski effect of electron distribution on roughened surfaces.[68] According to the Smoluchowski effect, electrons flow from the "hills" into the "valleys" on the stepped surface, resulting in a net positive charge on the "hills" and a negative charge in the "valleys". Therefore, a homogeneous surface charge density assumed in our model is invalid for stepped surfaces; instead, the heterogeneity of surface charge density must be considered. On stepped surfaces, the HPRR can occur on the positively charged "hills", which explains the experimental phenomena observed by Briega-Martos et al.[45]

Overview of various surface charge effects in electrocatalysis

This section is aimed at putting this work in a wider context. Several surface charge effects in electrocatalysis have been proposed, including (a) Frumkin effects, (b) field-dependent adsorption energy, and (c) interfacial solvation effects. In what follows, the basic idea of each surface charge effect is introduced, followed with a comparison between these surface charge effects and the one presented here.

The Frumkin effects describe how the surface charge modifies the electric potential and concentration of ionic reactant(s) in the local reaction zone. In addition to the substantial contribution of the Frumkin school, other principal advances include Gierst's consideration of ion pairs,[69] Parsons's study on the effect of specific adsorption,[70] the consideration of discreteness-of-charge effects notably by Levine and Fawcett,[71] and the extension of a reaction plane to a reaction volume by Nazmutdinov et al.[72]

The field-dependent adsorption effect describes impact of the interfacial electric field on the adsorption energy of reaction intermediates bearing an internal dipole moment.[66, 73-75] As a result, the surface charge modifies the Gibbs free energy and, based on the Brønsted−Evans−Polanyi relation, the activation energy of elementary reaction steps involving such adsorbed intermediates.

The interfacial solvation environment affects both energetic parameters (the activation barrier) and dynamic parameters (*e.g.*, the barrier crossing frequency) in the expression for the rate of electron transfer.[76] As the solvent orientation is determined by the local electric field, the interfacial solvation environment is modulated definitely by the surface charge. For instance, the solvent reorganization energy λ has shown to decrease as the reactant approaches closer to the electrode surface,[30, 31] and as the electrode surface gets more charged.[29]

In comparison, these surface charge effects have different foci. The Frumkin effects are most pronounced for redox reaction of multivalent ions, such as $S_2O_8^{2-}$. As a recent example, cation effects on the oxygen evolution reaction (OER) at metal oxides are interpreted by the virtue of the Frumkin effects.[77] Specifically, the negative charge on the metal oxide causes cation overcrowding and decreased concentration of OH^- in the EDL. Consequently, the OER activity decreases in the presence of cations with a larger effective size. The field-dependent adsorption effect is important for interfacial electrochemical and chemical reactions involving adsorbed intermediates with a dipole moment, for instance, $*CO_2$ and *OCCO in the carbon dioxide reduction.[4, 78] Surface charge effects via modulating the interfacial solvation should be important for all interfacial electron transfer reactions. However, it has been less considered in previous studies of EDL effects in electrocatalysis. Part of the reason might be that the solvation environment plays no explicit role in the

phenomenological Butler-Volmer equation which has been widely used to describe the kinetics of elementary electron transfer steps.

In contrast, the surface charge presented in this work describes that the surface charge modulates the location of the reaction plane, rather than assuming a fixed reaction plane as previously. Such a surface charge effect is not limited to the specific case considered here. In fact, a varying distance between the electrode and the Stern layer modulated by the surface charge density has been found in AIMD studies.[36, 37]

Conclusion

We have presented a theoretical study on the surface charge effect on H_2O_2 redox reactions at Pt(111), combining AIMD simulations, microkinetic analysis, and continuum modelling of the EDL. The AIMD simulations show that the O-O bond of the hydrogen peroxide molecule (the reactant) is, statistically speaking, located at a larger distance away from the platinum surface with negative surface charge, compared to the case with positive surface charge. As the electronic interaction strength decays exponentially with distance, we expect that the activation barrier of breaking the oxygen-oxygen bond of the hydrogen peroxide molecule is higher, resulting in the abnormal experimental observation that the reduction current is suppressed with decreasing the electrode potential.

Built upon this postulate, a microkinetic-double layer model provides a detailed interpretation scheme for the polarization curves of this model system has been provided. Below 0.2 V_{RHE}, the convergence of polarization curves at different pHs into a single curve is due to the site-blocking effect of hydrogen adsorption that is near thermodynamic equilibrium and is pH-independent on the RHE scale. In the potential region of 0.2-0.6 V_{RHE}, the suppression of HPRR is caused by the negative surface charge. Particularly, our AIMD simulations reveal that the negative surface charge on Pt(111) repels the O-O bond of H_2O_2 farther away from the electrode surface, resulting in a higher activation barrier for breaking the O-O bond. This surface charge effect explains why the suppression occurs at higher potentials for higher solution pHs, and

is more significant in the presence of cations of smaller effective size. The benchmark model that considers Frumkin effects but neglects this surface charge effect is unable to reproduce the pH-dependent suppression of the HPRR in the region 3. In the potential region of 0.6-0.9 V_{RHE}, the net reduction current is nearly pH-independent, due to the ultrafast kinetics of OH_{ad} adsorption at Pt(111). Under equilibrium, the HPOR should be pH-independent on the RHE scale, as both elementary steps of the HPOR are proton-coupled electron transfer steps. The decrease in the net oxidation current at potentials above 0.9 V_{RHE}, at higher pHs represents an evidence for the importance of nonequilibrium microkinetics.

ASSOCIATED CONTENT

Supporting Information.

Following materials are included in this supporting information file: AIMD simulation details; supporting figures; Matlab scripts of model calculation. This material is available free of charge via the Internet at http://pubs.acs.org.

AUTHOR INFORMATION

Corresponding Author

* jun.huang@uni-ulm.de (J.H.), and juan.feliu@ua.es (J.F.)

Author Contributions

The manuscript was written through contributions of all authors.

ACKNOWLEDGMENT

J.H. acknowledges the financial support for a Europe Research Stay at Alicante University from the Alexander von Humboldt Foundation, and National Natural Science Foundation of China under the grant number of 21802170. Computer time provided by the state of Baden-Württemberg through bwHPC and the German Research Foundation (DFG) through grant no INST 40/575-1 FUGG (JUSTUS 2 cluster) are gratefully acknowledged. This work contributes to the research performed at CELEST (Center for Electrochemical

Energy Storage Ulm-Karlsruhe). J.M.F and V.C. acknowledge financial support from Ministerio de Ciencia e Innovación (Project PID2019-105653GB-100) and Generalitat Valenciana (Project PROMETEO/2020/063).

REFERENCES

[1] A. Kozawa, Effects of anions and cations on oxygen reduction and oxygen evolution reactions on platinum electrodes, Journal of Electroanalytical Chemistry (1959), 8 (1964) 20-39.

[2] D. Strmcnik, K. Kodama, D. van der Vliet, J. Greeley, V.R. Stamenkovic, N.M. Marković, The role of non-covalent interactions in electrocatalytic fuel-cell reactions on platinum, Nature Chemistry, 1 (2009) 466-472.

[3] A.C. Garcia, T. Touzalin, C. Nieuwland, N. Perini, M.T.M. Koper, Enhancement of Oxygen Evolution Activity of Nickel Oxyhydroxide by Electrolyte Alkali Cations, Angewandte Chemie International Edition, 58 (2019) 12999-13003.

[4] S. Ringe, E.L. Clark, J. Resasco, A. Walton, B. Seger, A.T. Bell, K. Chan, Understanding cation effects in electrochemical CO2 reduction, Energy & Environmental Science, 12 (2019) 3001-3014.

[5] B. Deng, M. Huang, X. Zhao, S. Mou, F. Dong, Interfacial Electrolyte Effects on Electrocatalytic CO2 Reduction, ACS Catalysis, 12 (2022) 331-362.

[6] P. Sebastián-Pascual, Y. Shao-Horn, M. Escudero-Escribano, Toward understanding the role of the electric double layer structure and electrolyte effects on well-defined interfaces for electrocatalysis, Current Opinion in Electrochemistry, 32 (2022) 100918.

[7] S.-J. Shin, D.H. Kim, G. Bae, S. Ringe, H. Choi, H.-K. Lim, C.H. Choi, H. Kim, On the importance of the electric double layer structure in aqueous electrocatalysis, Nature Communications, 13 (2022) 174.

[8] K. Chan, A few basic concepts in electrochemical carbon dioxide reduction, Nature Communications, 11 (2020) 5954.

[9] J. Huang, Surface Charging Behaviors of Electrocatalytic Interfaces with Partially Charged Chemisorbates, Current Opinion in Electrochemistry, (2022) 100938.

[10] A. Frumkin, Wasserstoffüberspannung und Struktur der Doppelschicht, Zeitschrift für Physikalische Chemie, 1933, pp. 121.

[11] L.-L. Zhang, C.-K. Li, J. Huang, A Beginners' Guide to Modelling of Electric Double Layer Under Equilibrium, Nonequilibrium and Ac Conditions, Journal of Electrochemistry, (2021) 0-.

[12] A.N. Frumkin, N.V. Nikolaeva-Fedorovich, N.P. Berezina, K.E. Keis, The electroreduction of the S2O82− anion, Journal of Electroanalytical Chemistry and Interfacial Electrochemistry, 58 (1975) 189-201.

[13] V. Climent, J.M. Feliu, Thirty years of platinum single crystal electrochemistry, Journal of Solid State Electrochemistry, 15 (2011) 1297.

[14] V. Climent, J. Feliu, Single Crystal Electrochemistry as an In Situ Analytical Characterization Tool, Annual Review of Analytical Chemistry, 13 (2020) 201-222.

[15] J. Clavilier, The role of anion on the electrochemical behaviour of a {111} platinum surface; an unusual splitting of the voltammogram in the hydrogen region, Journal of Electroanalytical Chemistry and Interfacial Electrochemistry, 107 (1980) 211-216.

[16] J. Clavilier, R. Faure, G. Guinet, R. Durand, Preparation of monocrystalline Pt microelectrodes and electrochemical study of the plane surfaces cut in the direction of the {111} and {110} planes, Journal of Electroanalytical Chemistry and Interfacial Electrochemistry, 107 (1980) 205-209.

[17] A.M.A. El-Halim, K. Jüttner, W.J. Lorenz, The electrocatalytical influence of thallium and lead underpotential adsorbates at silver single-crystal surfaces on the reduction processes of quinone, persulphate and protons, Journal of Electroanalytical Chemistry and Interfacial Electrochemistry, 106 (1980) 193-207.

[18] Z. Samec, A.M. Bittner, K. Doblhofer, Electrocatalytic reduction of peroxodisulfate anion on Au(111) in acidic aqueous solutions, Journal of Electroanalytical Chemistry, 409 (1996) 165-173.

[19] Z. Samec, A.M. Bittner, K. Doblhofer, Origin of electrocatalysis in the reduction of peroxodisulfate on gold electrodes, Journal of Electroanalytical Chemistry, 432 (1997) 205-214.

[20] E. Lust, R. Truu, K. Lust, Electroreduction of peroxodisulfate anion at Bi(111) single-crystal plane electrode, Russian Journal of Electrochemistry, 36 (2000) 1195-1202.

[21] V. Climent, M.D. Maciá, E. Herrero, J.M. Feliu, O.A. Petrii, Peroxodisulphate reduction as a novel probe for the study of platinum single crystal/solution interphases, Journal of Electroanalytical Chemistry, 612 (2008) 269-276.

[22] R. Martínez-Hincapié, V. Climent, J.M. Feliu, Peroxodisulfate reduction as a probe to interfacial charge, Electrochemistry Communications, 88 (2018) 43-46.

[23] V. Briega-Martos, E. Herrero, J.M. Feliu, Pt(hkl) surface charge and reactivity, Current Opinion in Electrochemistry, (2019).

[24] R. Martínez-Hincapié, V. Climent, J.M. Feliu, New probes to surface free charge at electrochemical interfaces with platinum electrodes, Current Opinion in Electrochemistry, 14 (2019) 16-22.

[25] J. Huang, J. Zhang, M. Eikerling, Unifying theoretical framework for deciphering the oxygen reduction reaction on platinum, Physical Chemistry Chemical Physics, 20 (2018) 11776-11786.

[26] D. Zhou, J. Wei, Z.-D. He, M.-L. Xu, Y.-X. Chen, J. Huang, Combining Single Crystal Experiments and Microkinetic Modeling in Disentangling Thermodynamic, Kinetic, and Double-Layer Factors Influencing Oxygen Reduction, The Journal of Physical Chemistry C, 124 (2020) 13672-13678.

[27] l. Zhang, J. Cai, Y. Chen, J. Huang, Modelling electrocatalytic reactions with a concerted treatment of multistep electron transfer kinetics and local reaction conditions, Journal of Physics: Condensed Matter, (2021).

[28] S. Ringe, C.G. Morales-Guio, L.D. Chen, M. Fields, T.F. Jaramillo, C. Hahn, K. Chan, Double layer charging driven carbon dioxide adsorption limits the rate of electrochemical carbon dioxide reduction on Gold, Nature Communications, 11 (2020) 33.

[29] J. Huang, Mixed quantum-classical treatment of electron transfer at electrocatalytic interfaces: Theoretical framework and conceptual analysis, The Journal of Chemical Physics, 153 (2020) 164707.

[30] R.E. Bangle, J. Schneider, E.J. Piechota, L. Troian-Gautier, G.J. Meyer, Electron Transfer Reorganization Energies in the Electrode–Electrolyte Double Layer, Journal of the American Chemical Society, 142 (2020) 674-679.

[31] A.M. Limaye, W. Ding, A.P. Willard, Understanding attenuated solvent reorganization energies near electrode interfaces, The Journal of Chemical Physics, 152 (2020) 114706.

[32] S. Sakong, K. Forster-Tonigold, A. Groß, The structure of water at a Pt(111) electrode and the potential of zero charge studied from first principles, J. Chem. Phys., 144 (2016) 194701.

[33] J. Le, M. Iannuzzi, A. Cuesta, J. Cheng, Determining Potentials of Zero Charge of Metal Electrodes versus the Standard Hydrogen Electrode from Density-Functional-Theory-Based Molecular Dynamics, Phys. Rev. Lett., 119 (2017) 016801.

[34] S. Sakong, A. Groß, The electric double layer at metal-water interfaces revisited based on a charge polarization scheme, J. Chem. Phys., 149 (2018) 084705.

[35] P. Li, J. Huang, Y. Hu, S. Chen, Establishment of the Potential of Zero Charge of Metals in Aqueous Solutions: Different Faces of Water Revealed by Ab Initio Molecular Dynamics Simulations, The Journal of Physical Chemistry C, 125 (2021) 3972-3979.

[36] J.-B. Le, Q.-Y. Fan, J.-Q. Li, J. Cheng, Molecular origin of negative component of Helmholtz capacitance at electrified Pt(111)/water interface, Science Advances, 6 (2021) eabb1219.

[37] S. Sakong, A. Groß, Water structures on a Pt(111) electrode from ab initio molecular dynamic simulations for a variety of electrochemical conditions, Physical Chemistry Chemical Physics, 22 (2020) 10431-10437.

[38] T. Iwasita, X. Xia, Adsorption of water at Pt(111) electrode in HClO4 solutions. The potential of zero charge, Journal of Electroanalytical Chemistry, 411 (1996) 95-102.

[39] C.-Y. Li, J.-B. Le, Y.-H. Wang, S. Chen, Z.-L. Yang, J.-F. Li, J. Cheng, Z.-Q. Tian, In situ probing electrified interfacial water structures at atomically flat surfaces, Nature Materials, 18 (2019) 697-701.

[40] I. Katsounaros, W.B. Schneider, J.C. Meier, U. Benedikt, P.U. Biedermann, A.A. Auer, K.J.J. Mayrhofer, Hydrogen peroxide electrochemistry on platinum: towards understanding the oxygen reduction reaction mechanism, Physical Chemistry Chemical Physics, 14 (2012) 7384-7391.

[41] A.M. Gómez-Marín, K.J.P. Schouten, M.T.M. Koper, J.M. Feliu, Interaction of hydrogen peroxide with a Pt(111) electrode, Electrochemistry Communications, 22 (2012) 153-156.

[42] Y.L. Zheng, D. Mei, Y.-X. Chen, S. Ye, The redox reaction of hydrogen peroxide at an Au(100) electrode: Implications for oxygen reduction kinetics, Electrochemistry Communications, 39 (2014) 19-21.

[43] E. Sitta, J.M. Feliu, The Role of PtOH on H2O2 Interactions with Platinum Surfaces in an Electrochemical Environment, ChemElectroChem, 1 (2014) 55-58.

[44] R. Rizo, J.M. Feliu, E. Herrero, New insights into the hydrogen peroxide reduction reaction and its comparison with the oxygen reduction reaction in alkaline media on well-defined platinum surfaces, Journal of Catalysis, 398 (2021) 123-132.

[45] V. Briega-Martos, E. Herrero, J.M. Feliu, Hydrogen peroxide and oxygen reduction studies on Pt stepped surfaces: Surface charge effects and mechanistic consequences, Electrochimica Acta, 334 (2020) 135452.

[46] Y. Zheng, W. Chen, X.-Q. Zuo, J. Cai, Y.-X. Chen, The kinetics of the oxidation and reduction of H2O2 at a Pt electrode: A differential electrochemical mass spectrometric study, Electrochemistry Communications, 73 (2016) 38-41.

[47] V. Briega-Martos, E. Herrero, J.M. Feliu, The inhibition of hydrogen peroxide reduction at low potentials on Pt(111): Hydrogen adsorption or interfacial charge?, Electrochemistry Communications, 85 (2017) 32-35.

[48] U.A. Paulus, T.J. Schmidt, H.A. Gasteiger, R.J. Behm, Oxygen reduction on a high-surface area Pt/Vulcan carbon catalyst: a thin-film rotating ring-disk electrode study, Journal of Electroanalytical Chemistry, 495 (2001) 134-145.

[49] T. Pajkossy, D.M. Kolb, Double layer capacitance of the platinum group metals in the double layer region, Electrochemistry Communications, 9 (2007) 1171-1174.

[50] K. Ojha, N. Arulmozhi, D. Aranzales, M.T.M. Koper, Double Layer at the Pt(111)–Aqueous Electrolyte Interface: Potential of Zero Charge and Anomalous Gouy–Chapman Screening, Angewandte Chemie International Edition, 59 (2020) 711-715.

[51] R. Martínez-Hincapié, P. Sebastián-Pascual, V. Climent, J.M. Feliu, Exploring the interfacial neutral pH region of Pt(111) electrodes, Electrochemistry Communications, 58 (2015) 62-64.

[52] J. Le, A. Cuesta, J. Cheng, The structure of metal-water interface at the potential of zero charge from density functional theory-based molecular dynamics, Journal of Electroanalytical Chemistry, 819 (2018) 87-94.

[53] F.D. Lewis, J. Liu, W. Weigel, W. Rettig, I.V. Kurnikov, D.N. Beratan, Donor-bridge-acceptor energetics determine the distance dependence of electron tunneling in DNA, 99 (2002) 12536-12541.

[54] A. Bruix, J.T. Margraf, M. Andersen, K. Reuter, First-principles-based multiscale modelling of heterogeneous catalysis, Nature Catalysis, 2 (2019) 659-670.

[55] A. Salimi, C.E. Banks, R.G. Compton, Ultrasonic effects on the electro-reduction of oxygen at a glassy carbon anthraquinone-modified electrode. The Koutecky–Levich equation applied to insonated electro-catalytic reactions, Physical Chemistry Chemical Physics, 5 (2003) 3988-3993.

[56] J.K. Nørskov, J. Rossmeisl, A. Logadottir, L. Lindqvist, J.R. Kitchin, T. Bligaard, H. Jónsson, Origin of the Overpotential for Oxygen Reduction at a Fuel-Cell Cathode, The Journal of Physical Chemistry B, 108 (2004) 17886-17892.

[57] J. Huang, Hybrid density-potential functional theory of electric double layers, Electrochimica Acta, 389 (2021) 138720.

[58] J. Huang, Surface charging behaviors of electrocatalytic interfaces with partially charged chemisorbates, Current Opinion in Electrochemistry, 33 (2022) 100938.

[59] A.V. Usha, G. Atkinson, The effect of pressure on the dissociation constant of hydrofluoric acid and the association constant of the NaF ion pair at 25°C, Journal of Solution Chemistry, 21 (1992) 477-488.

[60] A. Tjell, K. Almdal, Diffusion rate of hydrogen peroxide through water-swelled polyurethane membranes, Sensing and Bio-Sensing Research, 21 (2018) 35-39.

[61] J.O.M. Bockris, M.A.V. Devanathan, K. Müller, On the structure of charged interfaces, Proc. Roy. Soc. A, 274 (1963) 55-79.

[62] M.J. Eslamibidgoli, M.H. Eikerling, Electrochemical Formation of Reactive Oxygen Species at Pt (111)—A Density Functional Theory Study, ACS Catalysis, 5 (2015) 6090-6098.

[63] J. Huang, A. Malek, J. Zhang, M.H. Eikerling, Non-monotonic Surface Charging Behavior of Platinum: A Paradigm Change, The Journal of Physical Chemistry C, 120 (2016) 13587-13595.

[64] W. Schmickler, On the Theory of Electrocatalysis, in: K. Uosaki (Ed.) Electrochemical Science for a Sustainable Society: A Tribute to John O'M Bockris, Springer International Publishing, Cham, 2017, pp. 95-111.

[65] V. Briega-Martos, F.J. Sarabia, V. Climent, E. Herrero, J.M. Feliu, Cation Effects on Interfacial Water Structure and Hydrogen Peroxide Reduction on Pt(111), ACS Measurement Science Au, (2021).

[66] M.M. Waegele, C.M. Gunathunge, J. Li, X. Li, How cations affect the electric double layer and the rates and selectivity of electrocatalytic processes, The Journal of Chemical Physics, 151 (2019) 160902.

[67] F.J. Sarabia, P. Sebastián, V. Climent, J.M. Feliu, New insights into the Pt(hkl)-alkaline solution interphases from the laser induced temperature jump method, Journal of Electroanalytical Chemistry, 872 (2020) 114068.

[68] R. Smoluchowski, Anisotropy of the Electronic Work Function of Metals, Physical Review, 60 (1941) 661-674.

[69] L. Gierst, L. Vandenberghen, E. Nicolas, A. Fraboni, Ion Pairing Mechanisms in Electrode Processes, Journal of The Electrochemical Society, 113 (1966) 1025.

[70] R. Parsons, The effect of specific adsorption on the rate of an electrode process, Journal of Electroanalytical Chemistry and Interfacial Electrochemistry, 21 (1969) 35-43.

[71] W.R. Fawcett, S. Levine, Discreteness-of-charge effects in electrode kinetics, Journal of Electroanalytical Chemistry and Interfacial Electrochemistry, 43 (1973) 175-184.

[72] R.R. Nazmutdinov, D.V. Glukhov, O.A. Petrii, G.A. Tsirlina, G.N. Botukhova, Contemporary understanding of the peroxodisulfate reduction at a mercury electrode, Journal of Electroanalytical Chemistry, 552 (2003) 261-278.

[73] J.K. Nørskov, F. Studt, F. Abild-Pedersen, T. Bligaard, Poisoning and Promotion of Catalysts, Fundamental Concepts in Heterogeneous Catalysis2014, pp. 150-154.

[74] V. Climent, N. García-Araez, J.M. Feliu, Influence of alkali cations on the infrared spectra of adsorbed (bi)sulphate on Pt(111) electrodes, Electrochemistry Communications, 8 (2006) 1577-1582.

[75] G. Hussain, L. Pérez-Martínez, J.-B. Le, M. Papasizza, G. Cabello, J. Cheng, A. Cuesta, How cations determine the interfacial potential profile: Relevance for the CO2 reduction reaction, Electrochimica Acta, 327 (2019) 135055.

[76] M.J. Weaver, Dynamical solvent effects on activated electron-transfer reactions: principles, pitfalls, and progress, Chemical Reviews, 92 (1992) 463-480.

[77] J. Huang, M. Li, M.J. Eslamibidgoli, M. Eikerling, A. Groß, Cation Overcrowding Effect on the Oxygen Evolution Reaction, JACS Au, 1 (2021) 1752-1765.

[78] J. Resasco, L.D. Chen, E. Clark, C. Tsai, C. Hahn, T.F. Jaramillo, K. Chan, A.T. Bell, Promoter Effects of Alkali Metal Cations on the Electrochemical Reduction of Carbon Dioxide, Journal of the American Chemical Society, 139 (2017) 11277-11287.

Table of Contents artwork